metals

MDPI

Article

Slag Modification in Reduction of Kiviniemi Ferrous Scandium Concentrates

Rita Kallio [1,*], Pekka Tanskanen [2], Eetu-Pekka Heikkinen [2], Tommi Kokkonen [2], Saija Luukkanen [1] and Timo Fabritius [2]

[1] Oulu Mining School, Faculty of Technology, University of Oulu, FI-90014 Oulu, Finland; saija.luukkanen@oulu.fi
[2] Process Metallurgy Research Group, Faculty of Technology, University of Oulu, FI-90014 Oulu, Finland; pekka.a.tanskanen@oulu.fi (P.T.); eetu.heikkinen@oulu.fi (E.-P.H.); tommi.kokkonen@oulu.fi (T.K.); timo.fabritius@oulu.fi (T.F.)
* Correspondence: rita.kallio@oulu.fi; Tel.: +358-50-526-6806

Abstract: Several research projects are currently focused on the search for new sources of scandium due to its expected increasing demand in advanced technology applications. The Kiviniemi Fe-Sc-enriched mafic intrusion is a potential primary source for Sc. According to the recent investigations on the FeO component reduction in the Kiviniemi magnetic Sc concentrate at various end temperatures, complete FeO reduction is achieved at the highest experimental temperature (1500 °C). However, efficient separation of metal from the Sc_2O_3-enriched slag is hindered by the high viscosity of the slag. In this study, investigations of the Kiviniemi-type concentrate reduction characteristics are complemented from three perspectives: (1) slag modification with CaF_2 and/or CaO to promote the reduction of the FeO component and metal separation, (2) reduction characteristics of the concentrates with a slightly different modal mineralogy and chemical composition, and (3) description of the main features of the progression of reduction at selected temperatures (950, 1050, 1150, 1250, and 1350 °C) with CaO addition. Both CaF_2 and CaO increase conversion rates at a lower temperature region and promote the separation of metal from the slag. High-temperature behavior of the concentrates used in this study is essentially similar, although the main reduction stage is initiated at a slightly higher temperature for concentrates with less amphibole and a higher amount of nonferrous gangue minerals. Only after the complete decomposition and melting of clinopyroxene and nonferrous minerals of the concentrate, the final reduction of the FeO component from the slag can take place.

Keywords: ferrous scandium concentrate; reduction; slag; modification

Citation: Kallio, R.; Tanskanen, P.; Heikkinen, E.-P.; Kokkonen, T.; Luukkanen, S.; Fabritius, T. Slag Modification in Reduction of Kiviniemi Ferrous Scandium Concentrates. *Metals* **2022**, *12*, 709. https://doi.org/10.3390/met12050709

Academic Editor: Alexander McLean

Received: 15 March 2022
Accepted: 18 April 2022
Published: 21 April 2022

1. Introduction

To meet the expected increasing demand of scandium, various primary and secondary scandium-rich resources are currently being investigated as potential new sources of this rare-earth element. The Kiviniemi mafic intrusion in Finland represents one of these potential new sources with a preliminary mineral resource estimation of 13.4 Mt and an average Sc grade of 163 g/t [1,2]. The main scandium-bearing minerals are ferrous amphibole and clinopyroxene [2–4]. Due to the paramagnetic nature of these minerals, a concentration stage involving low-intensity and high-gradient magnetic separation has been suggested for removing alkali-containing diamagnetic minerals with only negligible losses of Sc_2O_3 to the tailings [4]. With magnetic concentration, the total ferrous oxide load in the concentrate is inevitably high. Furthermore, due to the incorporation of scandium into the lattice of ferrous silicates, conventional beneficiation should be complemented with pyrometallurgical and/or hydrometallurgical methods. However, non-selective mobilization of Fe and Ti in hydrometallurgical processing imposes challenges to the purification and precipitation of suitable Sc products [5–8]. Moreover, as reported in the preliminary beneficiation study of Kiviniemi ferrodiorite [3], large quantities of acids are required, and large volumes of

byproducts are produced. Therefore, pyrometallurgical processing is suggested as a potential technique to decrease the amount of the ferrous oxide component in the concentrate prior to hydrometallurgical processing.

In the first part of our high-temperature studies, the results of reduction experiments of a ferrodiorite concentrate and characteristics of the products up to temperatures of 1500 °C were described [9]. The observed increase in the derivative conversion rates during the experiments initiated gradually from ~950 °C onwards with a sharp increase in the conversion rates between 1050 and 1170 °C and high rates until ~1250 °C. This was interpreted to signify the main melting and reduction stage, which continued as the formed FeO-containing slag reacted with graphite. Plagioclase and potassium feldspar are the main gangue minerals in the Kiviniemi concentrates [4]. In the plagioclase series, the liquidus temperature rises from the pure sodium endmember (albite 1118 °C) to the pure calcium endmember (anorthite 1550 °C) [10]; the plagioclase in the Kiviniemi samples is intermediate between the two endmembers, with its anorthite content being approximately 40 mol-% [2]. It is assumed that prior to complete melting of the partly reduced ferrous silicates and nonferrous gangue minerals, such as plagioclase, reduction reactions are hindered due to the formed product layers and remaining solid particles. Only after complete melting of the silicates and dissolution of unreduced FeO into the slag, the final FeO reduction can be achieved by carbon, accompanied by segregation and accumulation of metallic iron. Liquid-phase mass transfer of iron oxide has been regarded as the major factor in the rate of reduction of iron oxide by carbonaceous material in slags [11].

Viscosity as a measure of the internal friction of a fluid phase is one of the most important properties of metallurgical melts, directly affecting the kinetic conditions of the processes [12–14]. It is related to the internal structure of oxide melt and is very sensitive to changes in temperature, slag composition, and oxygen partial pressure [14,15]. Low viscosities improve the transfer of mass and heat, the solubility of slag formers and modifiers, and the separation of metal and slag. Network former SiO_2 has strong, highly covalent metal-oxygen bonds, leading to high liquid viscosities, whereas network transforming alkali and alkali earth oxides, such as Na_2O, K_2O, MgO, CaO, and other divalent oxides, such as MnO and FeO, break this network, thus decreasing the viscosity [12,13,16,17]. Amphoteric oxide Al_2O_3 may act either as a network former or transformer, depending on the composition of the slag system [17,18]. In the first part of our pyrometallurgical study, the viscosity of the slag was increased as the reduction reactions proceeded, decreasing the FeO content of the slag. This hindered the diffusion of the remaining FeO, which was particularly observed at lower final temperatures, also causing significant entrapment of small metal inclusions in the slag. Common techniques to lower the viscosity of the slag in metallurgical operations include the addition of CaO or CaF_2 [13,19,20]. It is generally recognized that F^- in the silicate melts is not coordinated with Si^{4+}, which means that CaF_2 is merely dissociated in the molten silicate [21]. As the slags are ionic in nature, containing both covalent and ionic bonds, and as the extent of polymerization varies with the metal oxide and flux contents in the slag, the viscosity of slags is extremely sensitive to the quality and quantity of ions and electrostatic interactions, as well as temperature [14,17]. In addition to viscosity, the slag composition with a suitable liquidus temperature—as based on the information from appropriate phase diagrams—is essential in industrial practices [17].

The experimental program in this second pyrometallurgical part of our study was designed to complement the characterization of the reduction behavior of Kiviniemi ferrous scandium concentrates from three perspectives: (1) modifying the slag composition with CaF_2 and/or CaO to lower the viscosity of the slag and promote the reduction of the FeO component with enhanced separation of metallic iron, (2) comparing the reduction of a variety of concentrates from various parts of the Kiviniemi mafic intrusion with selected CaF_2 and/or CaO doping, and (3) describing the main features of the progression of reduction with CaO addition at selected temperature intervals (950, 1050, 1150, 1250, and 1350 °C). The main aim is to produce a modified, improved slag composition to be used

in hydrometallurgical processing, document the progression of reduction, and provide fundamental information for the beneficiation scenarios of ferrous scandium concentrates.

2. Materials and Methods

Samples from three drill cores (R1, R2, and R3) from the Kiviniemi mafic intrusion were included in this study. Three adjacent or proximate drill core samples from four drill core intervals (altogether 12 individual samples) were combined into four composite samples. The composite samples are named R1, R2/u, R2/l, and R3 based on the drill cores they originate from; R2/u represents samples from the upper part and R2/l from the lower part of drill core R2 of the Kiviniemi intrusion [1,4]. The comminution procedure as well as magnetic separation with LIMS and SLon® 100 pulsating high-gradient magnetic separation (HGMS) at Metso Outotec laboratory in Pori, Finland are described in more detail in [4]. P_{80} values after comminution are 68, 85, 92, and 78 µm for R1, R2/u, R2/l, and R3 concentrates, respectively. The concentrates produced with SLon parameters (150 rpm and 1.0 T) with the highest Sc recovery and grade for each composite sample were selected for this study.

Concentrate bulk compositions were measured by Eurofins Labtium in Kuopio, Finland, using an accredited inductively coupled plasma optical emission spectrometry (ICP-OES) method (721P). Dry samples were pulverized to 100%—90 µm with a tungsten carbide mill at Oulu Mining School prior to sending for analysis. For ICP-OES analysis, a prepared pulp sample (0.2 g) is fused with anhydrous sodium peroxide in zirconium crucible by heating in electric furnace at 700°C for one hour. The melt is dissolved in hydrochloric acid. The final solution is diluted with water prior to instrumental analysis. The routine method entails the analysis of 27 elements by ICP-OES Thermo Electron ICAP 6500 Duo. Detection limits with quality control details are provided in Kallio et al., 2021 [4]. Polished vertical blocks (Ø 25 and 40 mm) of the concentrate grain mounts and samples after each high-temperature experiment were prepared for field emission scanning electron microscope (FESEM) and electron probe microanalyzer (EPMA) analysis, which were conducted at the Center of Material Analysis (CMA), University of Oulu. Polished blocks were coated with carbon prior to analyses. Data on modal mineralogy were acquired with INCAMineral software (version 5.05; Oxford Instruments, Oxford, Halifax, UK) and a Zeiss ULTRA Plus FESEM instrument (Oberkochen, Germany). The applied instrumental parameters were an acceleration voltage of 15 kV, beam current of 2.3 nA, and working distance of 8.3 mm. Postprocessing was conducted with GrainAlyzer software (Oxford Instruments, Oxford, Halifax, UK). A JEOL JXA-8530FPlus electron probe microanalyzer (JEOL Ltd., Tokyo, Japan) was employed to characterize mineral chemical compositions in concentrates as well as characteristics of the produced slag and metal, with the analytical conditions including an accelerating voltage of 15 kV, a beam current of 15 nA, and a beam diameter of 1–10 µm. The peak and background counting times were set at 10 s and 5 s, respectively, for all components. For Sc_2O_3, values of 30 s and 15 s were also tested. The matrix correction with the ZAF method (atomic number—absorption—fluorescence) was applied. The standards used with EPMA are reported in [9]. X-ray diffraction (XRD) was utilized to monitor the presence of crystalline phases at selected temperatures. A Rigaku SmartLab 9 kW XRD apparatus (Rikagu Ltd., Tokyo, Japan) with Co anode was used with 40 kV and 135 mA settings. Speed of acquisition was 4°/min with 0.02°/step and 2θ range of 10–130°. Data processing was performed with PDXL2 software and PDF-4 2022 database (Rikagu Ltd., Tokyo, Japan).

High-temperature experiments were conducted with a thermogravimetric (TG) furnace at the Laboratory of Process Metallurgy, University of Oulu. The experimental set-up is described in more detail in the first part of our pyrometallurgical study [9]. Ten grams of loose powders of the concentrate mix were prepared with calculated proportions of LIMS and SLon concentrates for each of these experiments. Based on the total ferrous oxide content of the concentrates, graphite powder (Thermo-Fisher Scientific, Karlsruhe, Germany, Alfa Aesar 40797 lot: 61100109) was mixed with the concentrate in correct proportions to

ensure the complete ferrous component reduction. Other chemicals used for modifying the slag composition were Alfa Aesar 33299 CaO (lot: P12F022), burned at 850 °C and stored in a desiccator, and Alfa Aesar 11055 CaF_2 (lot: Z27D012). Powders were pressed to the bottom of the graphite crucibles. In addition to the similar experimental procedure used in the first part of our pyrometallurgical study [9], quickly cooled samples at selected temperatures were included to investigate the progression of mineral reduction reactions at various stages. For these experiments, the gas composition was changed to 95% Ar and 5% H_2. After reaching the desired temperature in the TG furnace, the sample was raised to the upper, cooler part of the furnace, in which it was cooled with N_2 gas flow. The sample was taken out of the furnace after a few minutes of cooling. In total, the designed experimental program consists of 20 experiments, as presented in Table 1.

Table 1. High-temperature experimental TG program for Kiviniemi magnetic concentrates.

Focus of Experiment	No.	Sample	Target T (°C)	Isotherm, min	Additives
Effect of CaF_2 addition	1	R2/l	1450	120	5%C + 7%CaF_2
	2	R2/l	1450	120	5%C + 14%CaF_2
Effect of CaO addition	3	R2/l	1450	120	5%C + 5%CaO
	4	R2/l	1450	120	5%C + 10%CaO
Effect of CaO + CaF_2 addition	5	R2/l	1450	120	5%C + 7%CaF_2 + 5%CaO
Effect of concentrate quality, temperature and CaF_2 addition	6	R1	1500	120	5%C + 7%CaF_2
	7	R2/u	1500	120	5%C + 7%CaF_2
	8	R3	1500	120	5%C + 7%CaF_2
Effect of concentrate quality, temperature and CaO addition	9	R1	1500	120	5%C + 5%CaO
	10	R2/u	1500	120	5%C + 5%CaO
	11	R3	1500	120	5%C + 5%CaO
Effect of concentrate quality, temperature and CaF_2 + CaO addition	12	R1	1500	120	5%C + 7%CaF_2 + 5%CaO
	13	R2/u	1500	120	5%C + 7%CaF_2 + 5%CaO
	14	R3	1500	120	5%C + 7%CaF_2 + 5%CaO
Baseline with Ar + H_2 (5%)	15	R3	1500	10	~5%C + 5%CaO
Main features on the progression of reduction with CaO	16	R3	950	-	~5%C + 5%CaO
	17	R3	1050	-	~5%C + 5%CaO
	18	R3	1150	-	~5%C + 5%CaO
	19	R3	1250	-	~5%C + 5%CaO
	20	R3	1350	-	~5%C + 5%CaO

3. Results and Discussion

3.1. Characteristics of the Concentrates

Information on the concentrates produced with a combination of LIMS and SLon (150 rpm pulsation and 1.0 T applied magnetic induction) are presented in Table 2. Separate magnetic concentrates from LIMS and SLon were combined with correct mass proportions to produce a combined feed for high-temperature experiments to ensure the maximum possible recovery of both Sc_2O_3 and FeO.

Modal compositions of the combined concentrates used in our pyrometallurgical experiments are shown in Figure 1A. Their chemical compositions, as calculated based on ICP-OES results, are reported in Table 3. Feed chemical compositions based on the modal mineralogy and EPMA analyses are also provided as a reference. This comparison allows evaluation of the reliability of the process' mineralogical data, which are generally in agreement with the ICP-OES data. Chemical characteristics of the Kiviniemi intrusion include high Sc, Fe, Ti, and P content [2–4]. Despite deflecting apatite into the tailings in magnetic separation, the P_2O_5 grade in the concentrate remained at ~0.2–0.3 wt% (feed grade 0.6–0.74 wt%). FeO grades increased from the feed 19–23 wt% to concentrate 31–36 wt% while silica reduced from 42–47 wt% to 38–41 wt%, depending on the composite sample in question.

Table 2. Details of the selected concentrates processed with LIMS and SLon using composite samples R1, R2/u, R2/l (R2 upper and lower sample), and R3.

Drill Core Sample	R1	R2/u	R2/l	R3
Feed ppm Sc	150	210	170	180
LIMS mass %	9	9	10	8
LIMS Sc ppm	110	163	153	167
LIMS Sc recovery %	7	7	9	7
SLon MAGS mass %	55	62	65	52
SLon MAGS Sc ppm	230	310	250	310
SLon MAGS Sc recovery %	88	91	92	87
SLon Tailings mass %	45	39	35	49
SLon Tailings Sc ppm	40	50	40	50
TOTAL MAGS mass %	60	65	68	55
TOTAL MAGS Sc ppm	211	290	236	289
TOTAL MAGS Sc recovery %	89	91	93	88
TOTAL NMAGS mass %	40	35	32	45
TOTAL NMAGS Sc %	11	9	7	12

MAGS = magnetic concentrates, NMAGS = non-magnetic tailings.

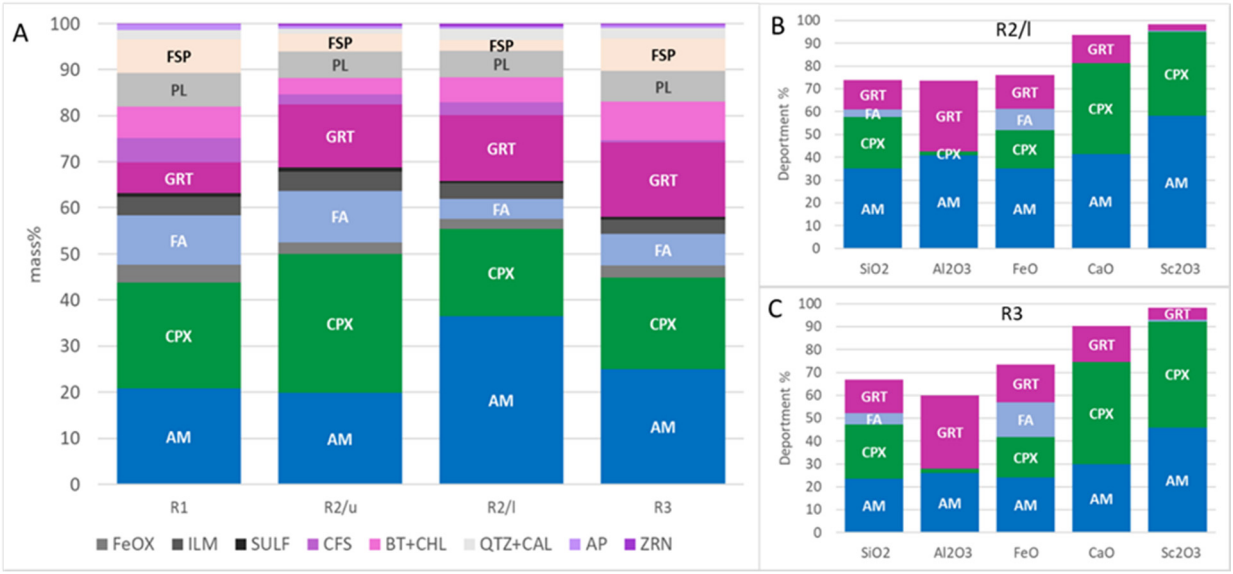

Figure 1. (**A**) Modal compositions of the concentrates used in pyrometallurgical experiments. Mineral abbreviations: AM = amphibole, CPX = clinopyroxene, FeOX = iron oxides (magnetite), FA = fayalite, ILM = ilmenite, SULF = sulfides, CFS = clinoferrosilite, GRT = garnet, BT + CHL = biotite + chlorite, PL = plagioclase, FSP = potassium feldspar, QTZ + CAL = quartz + calcite, AP = apatite, ZRN = zircon. (**B**,**C**) Deportment of SiO_2, Al_2O_3, FeO, CaO, and Sc_2O_3 in amphibole, clinopyroxene, fayalite, and garnet for concentrates R2/l and R3.

Although the feed samples represent the main lithology, with Sc-bearing amphibole and pyroxene having close to an average grade, there were differences in the amount of the main minerals between the feed composite samples and therefore also between produced concentrates. As indicated by Figure 1A, this was true particularly for the amounts of amphibole and clinopyroxene but also garnet and fayalite. Paramagnetic minerals, i.e., those with a ferrous component, accounted for 82–88 mass % of all the concentrates. Examples of the deportment of the main components—SiO_2, Al_2O_3, FeO, and CaO—as well as Sc_2O_3 within the four minerals (amphibole, clinopyroxene, fayalite, and garnet) in the R2/l and R3 concentrates are presented in Figure 1B,C. Further details on the deportment of the main components are provided in the electronic supplementary data (Table S1).

Mineralogically, Sc_2O_3 was mainly incorporated into the lattices of clinopyroxene and amphibole, though with varying amounts (Figure 1B,C). Garnet and amphibole accounted for most of the Al_2O_3 in the concentrates, whereas clinopyroxene introduced most of the CaO into the system, particularly in concentrate R2/u. Fayalite was a significant FeO-containing phase in concentrates R1 and R2/u. Compared with other concentrates, the R2/l concentrate had a significantly higher amount of amphibole.

Table 3. Chemical compositions of concentrates used in high-temperature experiments. Compositions calculated based on modal mineralogy are also provided for comparison. Sc_2O_3 presented in ppm, other oxides in wt%.

Sample	SiO_2	TiO_2	Al_2O_3	FeO	MnO	MgO	CaO	K_2O	P_2O_5	S	Sc_2O_3 (ppm)
R1 ICP-OES	39.8	3.08	8.33	32.7	0.61	1.81	7.99	1.52	0.32	0.28	324
R1 MODAL	39.3	2.68	7.84	33.1	0.58	1.62	8.57	1.43	0.48	0.32	289
R2/u ICP-OES	39.0	2.76	7.96	35.7	0.70	1.16	9.03	1.08	0.27	0.36	444
R2/u MODAL	39.2	2.72	7.80	33.1	0.66	1.16	9.92	0.96	0.25	0.34	441
R2/l ICP-OES	37.6	2.48	9.73	31.4	0.66	1.13	8.99	1.11	0.31	0.30	363
R2/l MODAL	40.3	2.52	9.27	31.5	0.76	1.11	9.70	0.59	0.22	0.19	380
R3 ICP-OES	40.7	2.45	10.1	31.2	0.59	0.97	8.71	1.63	0.22	0.28	444
R3 MODAL	39.7	2.07	9.88	29.9	0.59	0.95	8.88	1.54	0.21	0.20	380

3.2. Effects of Additions on Reduction of Concentrate R2/l

R2/l concentrate was used in the first part of the pyrometallurgical study [9]; R2/l concentrate with a slightly higher Sc_2O_3 grade and recovery was chosen as the first type of concentrate to test with selected additions. The details and results of experiments 1–5 conducted up to 1450 °C are presented in Table 4. The sum of the calculated mass of oxygen for FeO and P_2O_5, the calculated sum of hydroxyl in amphibole, biotite, and chlorite, and the mass of graphite are presented as a reference (Σ O + C + H_2O g). Hydroxyl removal from amphibole, biotite, and chlorite lattices was included assuming 1.86, 2.63, and 8.14 wt% of H_2O, respectively.

Table 4. Results of experiments 1–5 using the R2/l concentrate with various additives.

Sample	Experiment Number				
	1	2	3	4	5
Σ LIMS g	1.17	1.17	1.17	1.17	1.17
Slon g	8.83	8.83	8.83	8.83	8.83
C g	0.50	0.50	0.50	0.50	0.50
CaF_2 g	0.70	1.40	-	-	0.70
CaO g	-	-	0.50	1.00	0.50
Σ g	11.20	11.90	11.00	11.50	11.70
m_0 g	11.19	11.36	11.01	11.50	11.68
m_f g	9.05	8.91	9.35	9.82	9.61
Δm g	2.14	2.45	1.66	1.68	2.07
Δm %	19.12	21.57	15.08	14.61	17.72
Σ O + C + H_2O g	1.33	1.33	1.33	1.33	1.33

The calculation of the derivative conversion rates is explained in more detail in [9]. These rates exhibited acceleration at ~730–860 °C for samples with CaO doping, which did not appear as distinctly in the experiments with CaF_2 additions only (Figure 2). As presented in Figure 2, the main reaction stage was initiated with CaF_2- and/or CaO-doped R2/l samples at the same temperatures (~950 °C) as with non-doped samples, but with doping and less nonferrous gangue minerals, the reaction rates were faster with higher rates of conversion at lower temperatures. The CaO-doped samples appeared to have

their main peak in the derivative conversion rates at a slightly higher temperature (a rapid increase between 970–1020 °C) than with CaF_2 (950–990 °C). Furthermore, the derivative conversion rates exhibited another acceleration at ~1050–1120 °C for both types of doping at the main reduction stage, after which the rates sharply declined.

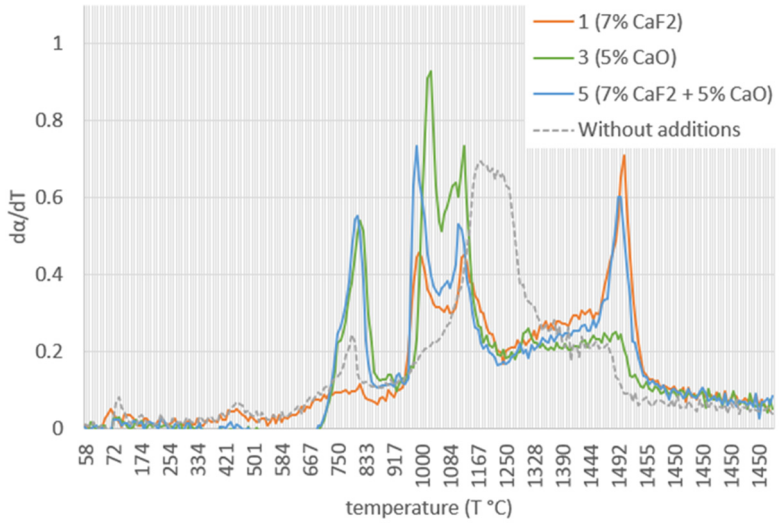

Figure 2. Derivative conversion curves for experiments 1, 3, and 5 using the R2/1 concentrate. The dotted line indicates a conversion curve obtained without any slag modification and with a higher amount of gangue minerals [9].

With CaF_2 additions, another significant increase in the conversion rates appeared approaching the final temperature (1450 °C) and particularly during the observed temperature overshoot (Figure 2). The differences between 5 and 10% additions of CaO seemed negligible according to the mass loss (Table 4), whereas the sample with the highest addition of CaF_2 (14%) exhibited the highest mass loss. This was interpreted to be caused by fluoride gas-forming reactions (Equation (1)) and increased silica reduction [22] and is one of the main reasons for the discrepancy between the calculated and measured mass losses (Table 4).

$$2CaF_2\ (slag) + SiO_2\ (slag) \rightarrow SiF_4\ (g) + 2CaO\ (slag) \quad (1)$$

Although CaF_2 has been widely used in the steel industry, it can be lost from industrial slags due to gas formation reactions, which increase with increasing temperature and set limits to the use of CaF_2 in industrial practice [22–24]. Depending on the temperature and composition of the slag, gaseous compounds such as KF, AlF_3 and NaF can also be emitted. Other reasons for the fluorspar substitution in the current industrial practices include refractory wear, environmental issues, and problems in the supply or availability of fluorspar [24].

Figure 3A,B show back-scattered electron images of slag produced without any additions and with 5% addition of CaO, respectively, in experiments with R2/1 concentrates at 1450 °C. The positive effect of the addition of network-transforming CaO on the reduction of the slag FeO component, as well as the separation of very small metal droplets in the slag, appeared to be obvious, with less metal retained in the slag. Figure 3A,B also present EPMA analysis points with corresponding results. The slag in both samples is visually homogeneous in back-scattered electron images but the analytical results reveal some variation, particularly in the SiO_2, FeO, and Sc_2O_3 contents without doping (Figure 3A), which was diminished with CaO doping (Figure 3B). A summary of the slag analytical data is provided in Table 5.

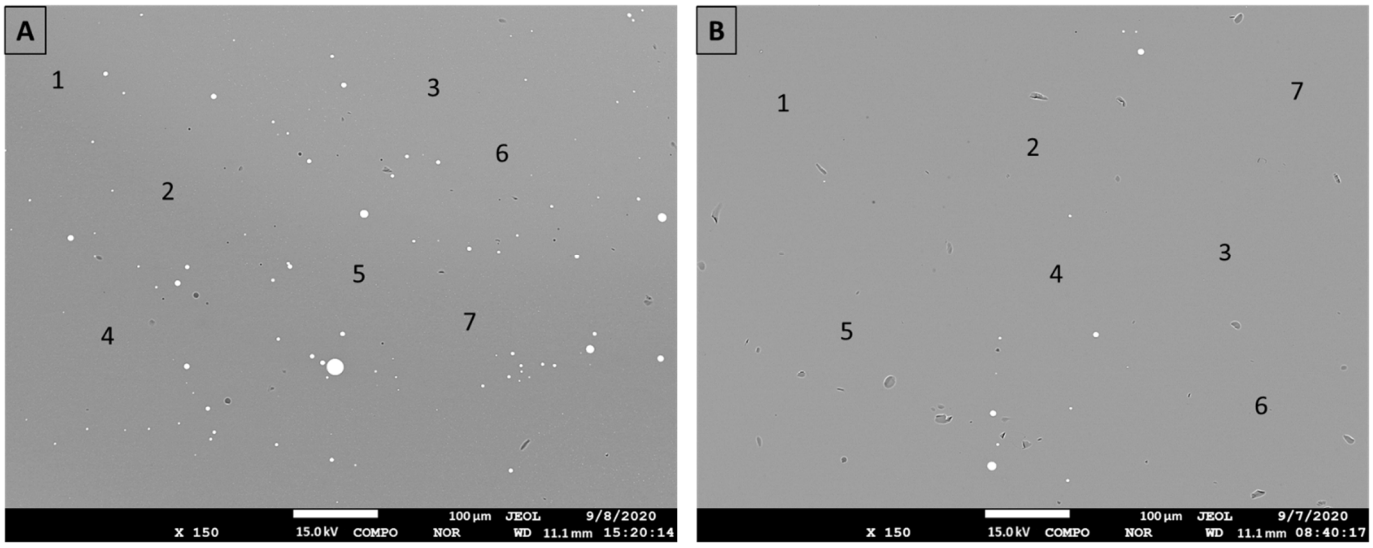

	SiO2	TiO2	Al2O3	FeO	MnO	MgO	CaO	Na2O	K2O	P2O5	ZrO2	Sc2O3	Total
1	59.13	3.12	14.34	1.72	0.70	1.56	12.96	2.17	1.67	0.01	0.69	270	98.10
2	59.10	3.02	14.29	1.58	0.76	1.43	12.74	2.24	1.72	0.00	0.54	410	97.45
3	58.00	3.02	14.00	3.14	0.79	1.46	12.78	2.22	1.64	0.00	0.72	400	97.79
4	59.95	2.97	14.67	0.95	0.72	1.48	12.49	2.27	1.79	0.00	0.69	360	98.02
5	59.47	3.01	14.55	1.29	0.75	1.47	12.56	2.33	1.71	0.00	0.74	670	97.95
6	57.87	3.01	14.06	3.02	0.79	1.52	13.06	2.18	1.63	0.02	0.65	280	97.86
7	59.59	2.92	14.46	1.45	0.78	1.46	12.56	2.26	1.76	0.00	0.66	530	97.95

	SiO2	TiO2	Al2O3	FeO	MnO	MgO	CaO	Na2O	K2O	P2O5	ZrO2	Sc2O3	Total
1	55.90	3.19	13.59	0.23	0.70	1.66	19.84	1.70	1.48	0.00	0.42	460	98.76
2	55.68	3.23	13.36	0.25	0.74	1.60	19.77	1.64	1.49	0.02	0.41	290	98.22
3	55.57	3.29	13.68	0.19	0.71	1.55	19.65	1.71	1.52	0.00	0.58	380	98.48
4	55.60	3.38	13.57	0.24	0.78	1.62	19.80	1.82	1.48	0.00	0.56	430	98.89
5	55.63	3.07	13.47	0.24	0.70	1.58	19.55	1.69	1.50	0.02	0.46	430	97.96
6	55.73	3.14	13.65	0.18	0.77	1.62	19.55	1.75	1.57	0.00	0.52	450	98.52
7	55.22	3.44	13.58	0.23	0.66	1.60	19.52	1.64	1.49	0.00	0.56	410	97.97

Figure 3. Back-scattered electron images of slag with EPMA analysis point locations and corresponding results in wt% after reduction experiments with the R2/1 concentrate conducted at 1450 °C. (**A**) Slag produced in the first part of our pyrometallurgical study without additions [9]. (**B**) Slag produced with 5% addition of CaO in this study.

Table 5. Average chemical compositions determined with EPMA for slags produced in reduction experiments 1–5; Sc_2O_3 ppm, other oxides wt%. n = number of analysis points.

Exp. No.	n	SiO_2	TiO_2	Al_2O_3	FeO	MnO	MgO	CaO	Na_2O	K_2O	P_2O_5	ZrO_2	Sc_2O_3	F
1	14	52.48	2.73	13.88	0.16	0.61	1.64	20.85	1.70	1.43	0.01	0.50	434	3.71
SD	-	0.20	0.18	0.11	0.44	0.03	0.05	0.22	0.04	0.02	0.01	0.06	91	0.07
2	14	47.63	2.27	13.13	0.04	0.52	1.55	26.80	1.47	1.12	0.01	0.50	366	6.23
SD		0.27	0.11	0.07	0.02	0.03	0.04	0.12	0.05	0.03	0.01	0.05	92	0.09
3	14	55.48	3.24	13.54	0.22	0.74	1.61	19.75	1.69	1.50	0.00	0.50	399	0.00
SD	-	0.23	0.11	0.11	0.03	0.04	0.04	0.16	0.05	0.02	0.01	0.09	89	0.00
4	13	51.82	3.11	12.59	0.13	0.68	1.52	24.92	1.52	1.37	0.01	0.45	420	0.00
SD	-	0.31	0.14	0.08	0.04	0.04	0.10	0.14	0.04	0.02	0.01	0.04	159	0.00
5	13	49.42	2.63	12.88	0.05	0.57	1.53	25.79	1.49	1.26	0.00	0.47	436	3.83
SD	-	0.27	0.08	0.12	0.03	0.05	0.02	0.17	0.06	0.02	0.01	0.03	107	0.05

According to the EPMA data (provided in electronic supplementary Table S2), CaF_2 addition promoted the reduction of SiO_2 and solution of silicon to ferrite. None of the metal analyses provided Sc contents above the detection limit (100 ppm Sc). Titanium carbide (TiC) formation was occasionally observed on the borders of graphite and ferrite. Metal analyses did not indicate the presence of Fe_3C. Figure 4 presents an overview of the characteristics of large metal accumulation after the experiment with 10% addition of CaO, with a close-up of the texture and EPMA point analytical data. The black areas in the back-scattered electron images represent graphite and the brightest phase is ferrite while the intermediate grey color represents steadite, the eutectic of ferrite and iron phosphide (Fe_3P). It solidifies during cooling from the liquid as the last constituent at the grain boundaries [25].

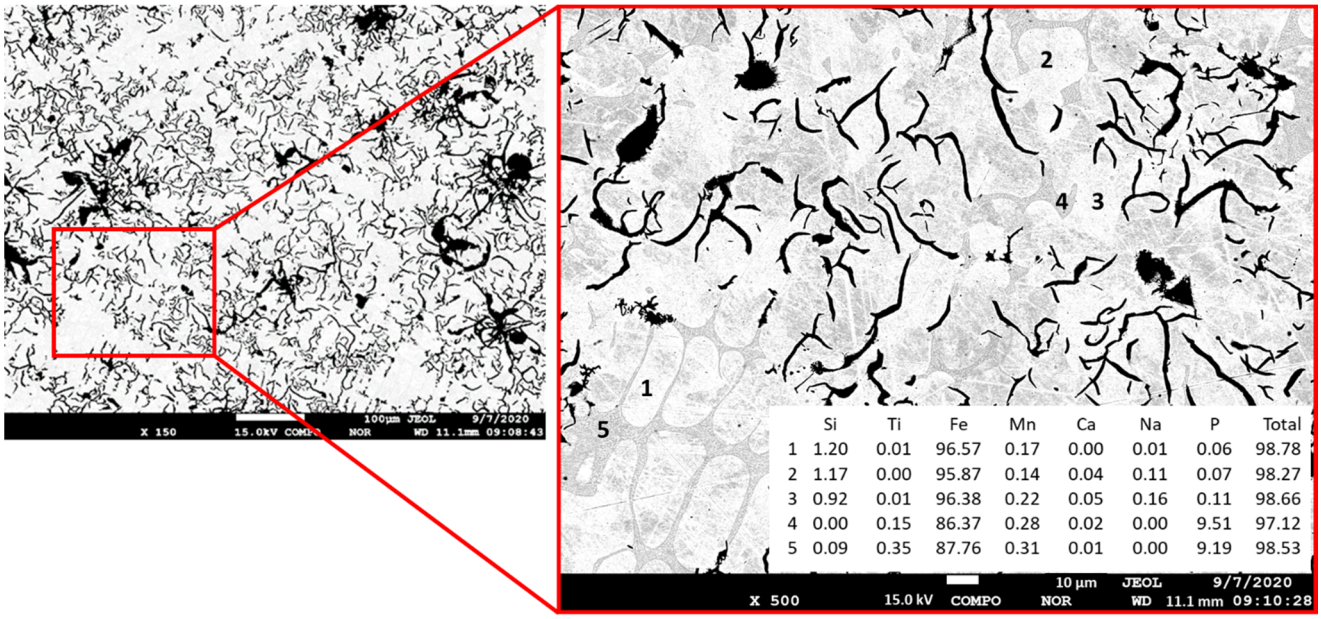

Figure 4. Example of large metal accumulation produced after reducing concentrate R2/l with 10% CaO addition. EPMA data on metal concentrations from points 1–5 expressed in wt%.

3.3. Comparison of Concentrate Quality with Selected Additions

Experiments 6–14 (Table 1) were conducted to compare the high-temperature properties and behavior of concentrates R1, R2/u, and R3, having differences in their modal mineralogy (Figure 1). Additions of 7% CaF_2, 5% CaO, and a combination of both of these two were used. The final isotherm was changed to the highest possible one in the TG furnace (1500 °C) to further improve the separation of small metal inclusions from the slag (Figure 3). Details of the feed materials and experimental results are presented in Table 6.

Table 6. Results of experiments 6–14 conducted up to 1500 °C with R1, R2/u, and R3 concentrates.

Exp. No.	6	7	8	9	10	11	12	13	14
Sample	R1	R2/u	R3	R1	R2/u	R3	R1	R2/u	R3
Σ LIMS g	1.59	1.39	1.44	1.59	1.39	1.44	1.59	1.39	1.44
Slon g	8.41	8.62	8.56	8.41	8.62	8.56	8.41	8.62	8.56
C g	0.50	0.50	0.50	0.50	0.50	0.50	0.50	0.50	0.50
CaF_2 g	0.70	0.70	0.70	-	-	-	0.70	0.70	0.70
CaO g	-	-	-	0.50	0.50	0.50	0.50	0.50	0.50
Σ g	11.20	11.21	11.20	11.00	11.01	11.00	11.70	11.71	11.70
m0 g	11.17	11.17	11.16	10.97	10.99	10.99	11.68	11.71	11.67
mf g	8.68	8.62	8.59	9.04	9.06	8.95	9.23	9.28	9.16
Δm g	2.49	2.55	2.57	1.93	1.93	2.04	2.45	2.43	2.51
Δm (%)	22.29	22.83	23.03	17.59	17.56	18.56	20.98	20.75	21.51
Σ O + C + H_2O g	1.33	1.38	1.28	1.33	1.38	1.28	1.33	1.38	1.28

The obtained mass loss curves (Figure 5A) and derivative conversion rates (Figure 5B–D) exhibited essentially similar characteristics for the three concentrates under the same experimental conditions. Compared with the other concentrates, the R2/l concentrate used in the first part of our pyrometallurgical study [9] and in the first five experiments of this study contains a significantly higher amount of amphibole, which likely is the reason for the slightly lower temperature region for the higher conversion rates (Figures 2 and 5) initiating at ~950 °C. Although the main reduction stage appeared to initiate at a slightly higher temperature (~1000 °C), R1, R2/u, and R3 concentrates all exhibited higher rates

of conversion with both additions at a lower temperature region as compared to the R2/l concentrate without slag modification (Figure 5).

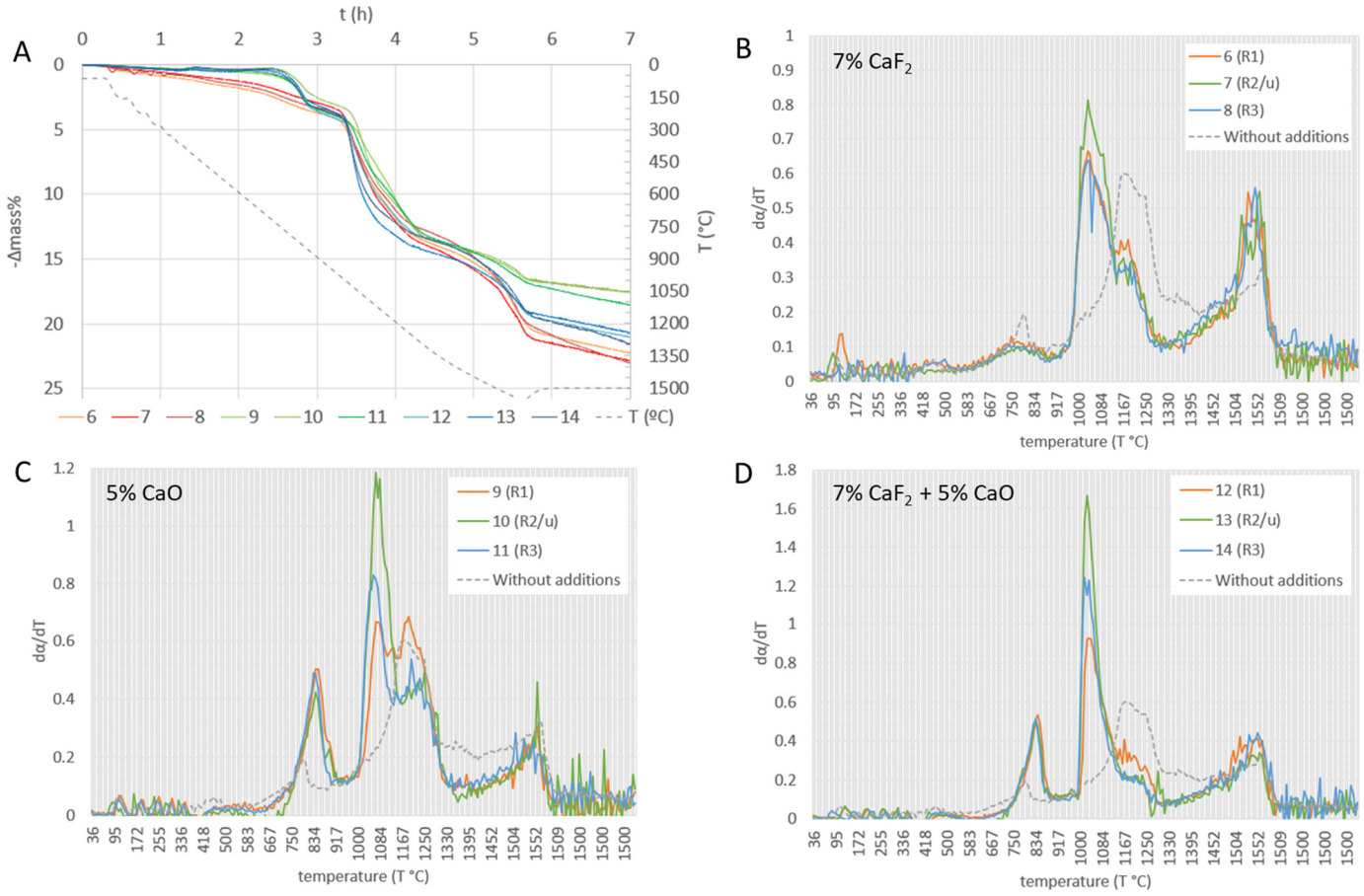

Figure 5. (**A**) Mass-loss curves for experiments 6–14, with all conducted using the same temperature program up to 1500 °C for R1, R2/u, and R3 concentrates. (**B**–**D**) Derivative conversion curves for experiments 6–8 (with 7% CaF_2), 9–11 (with 5% CaO), and 12–14 (with 7% CaF_2 + 5% CaO). Conversion rates for R2/l concentrate without additions shown as a reference [9].

The R2/u concentrate has the highest FeO content and exhibited the highest derivative conversion rates at the main stage of reduction reactions. Similar to the first set of experiments, the conversion rates with CaF_2 occurred at slightly lower temperatures than with CaO additions. Both additions alone exhibited a wider temperature region for higher rates of conversion, whereas with the combined and thus the highest amount of doping, the rate increased and decreased very sharply (Figure 5D), occurring within a narrower temperature range. This is interpreted to be caused by improved slag-forming reactions and slag characteristics due to a lower viscosity, which in turn enhances mass-transfer phenomena and allows faster reduction reactions within a narrower temperature interval. As observed in the previous and current set of experiments, with CaO additions at the low-temperature regime (<900 °C) in CO atmosphere, the reversed Boudouard reaction is likely to occur with the possibility of reaction with CaO, based on the mass loss curves and derivative conversion rates (Figures 2 and 5) [26].

Average slag compositions determined with EPMA are presented in Table 7. As mentioned earlier, the counting times were 10 s for peaks and 5 s for background for each element in the beginning of our analytical work. This was initially considered an appropriate compromise between a reasonable total analysis time, also considering the available WDS crystals and detectors. Regarding the electron microprobe analysis of trace elements (<1000 ppm) for phases that are stable under a dense electron beam, the detection

limit and precision could be decreased by using a higher acceleration voltage and beam current combined with a longer counting time [27]. Due to the observed high standard deviation for Sc_2O_3 in the first set of slag analyses for these samples (data provided in electronic supplementary Table S3), longer peak and background counting times were tested to improve the quality of the data; the counting times of 30 s for peaks and 15 s for background were set for Sc_2O_3 only, while the initial parameters were employed for other components. This lowered the standard deviation and provided results closer to the calculated values. More specific analysis of Sc_2O_3 with a higher acceleration voltage and beam current and/or a longer counting time might provide potential to lower the detection limit and standard deviation even further [28,29]. The calculated slag compositions listed in Table 7 are normalized, excluding FeO and P_2O_5 from the ICP-OES results and considering the applied doping. As an exception to other components, the Na_2O values were calculated based on modal mineralogy because the samples were subjected to the sodium peroxide fusion prior to ICP-OES analysis. The differences between the analyzed and calculated slag compositions are visualized in Figure 6, which is based on the percentage of the difference of EPMA analyzed values from calculated value to provide an indication of the extent of reduction for other slag components in addition to FeO and P_2O_5.

Table 7. Average chemical compositions determined with EPMA for slags produced in reduction experiments 6–14; Sc_2O_3 ppm, other oxides wt%. n = number of analysis points. Calc = calculated values based on ICP-OES data, excluding FeO and P_2O_5 components.

Exp. No.	n	SiO_2	TiO_2	Al_2O_3	FeO	MnO	MgO	CaO	Na_2O	K_2O	P_2O_5	ZrO_2	Sc_2O_3	F
6	20	53.17	2.71	12.80	0.03	0.52	2.83	20.74	1.42	2.02	0.01	0.12	389	3.78
SD	-	0.42	0.10	0.10	0.02	0.03	0.06	0.28	0.04	0.05	0.01	0.03	64	0.05
Calc.	-	54.76	4.24	11.46	0.00	0.83	2.47	17.76	1.40 *	2.09	0.00	-	446	4.56
7	20	54.04	2.30	12.16	0.03	0.64	1.85	22.53	1.17	1.46	0.01	0.38	604	3.73
SD	-	0.33	0.14	0.09	0.02	0.03	0.04	0.14	0.05	0.03	0.01	0.05	58	0.08
Calc.	-	54.69	3.87	11.17	0.00	0.98	1.63	19.66	1.24 *	1.52	0.00	-	623	4.72
8	20	52.71	2.31	14.99	0.03	0.49	1.44	20.90	1.54	2.09	0.01	0.16	559	3.76
SD	-	0.19	0.12	0.08	0.02	0.03	0.05	0.10	0.04	0.03	0.01	0.03	71	0.08
Calc.	-	54.50	3.28	13.57	0.00	0.79	1.30	18.28	1.25 *	2.19	0.00	-	595	4.46
9 **	20	56.27	4.39	12.32	0.09	0.70	2.74	19.68	1.52	2.16	0.01	0.12	381	0.00
SD	-	0.29	0.18	0.07	0.03	0.02	0.06	0.15	0.04	0.04	0.01	0.04	61	0.00
Calc.	-	57.45	4.45	12.03	0.00	0.88	2.61	18.57	1.41 *	2.19	0.00	-	468	
10 **	20	56.85	3.87	11.89	0.07	0.82	1.84	21.63	1.23	1.56	0.00	0.38	594	0.00
SD	-	0.24	0.13	0.08	0.03	0.04	0.04	0.09	0.05	0.03	0.01	0.03	49	0.00
Calc.	-	57.51	4.07	11.61	0.00	1.03	1.72	20.63	1.29 *	1.60	0.00	-	655	
11 **	20	55.74	3.43	14.58	0.10	0.65	1.45	20.04	1.61	2.24	0.00	0.16	542	0.00
SD	-	0.18	0.17	0.16	0.03	0.03	0.03	0.14	0.05	0.04	0.01	0.03	60	0.00
Calc.	-	57.07	3.44	14.21	0.00	0.83	1.36	19.09	1.31 *	2.29	0.00	-	623	
12	20	50.22	2.45	11.76	0.04	0.51	2.62	25.89	1.16	1.72	0.01	0.11	326	3.97
SD	-	0.17	0.12	0.08	0.02	0.04	0.03	0.13	0.03	0.02	0.01	0.02	59	0.07
Calc.	-	51.34	3.98	10.75	0.00	0.78	2.33	22.93	1.28 *	1.96	0.00	-	418	4.26
13	20	50.41	2.32	11.15	0.03	0.65	1.71	27.60	1.00	1.23	0.01	0.38	533	3.98
SD	-	0.15	0.09	0.08	0.02	0.04	0.04	0.13	0.03	0.03	0.01	0.03	52	0.05
Calc.	-	51.16	3.62	10.45	0.00	0.91	1.53	24.84	1.16 *	1.42	0.00	-	583	4.41
14	20	49.44	2.06	13.95	0.02	0.45	1.37	26.27	1.21	1.75	0.01	0.14	477	3.93
SD	-	0.22	0.10	0.04	0.02	0.03	0.04	0.11	0.04	0.03	0.01	0.03	47	0.08
Calc.	-	51.15	3.08	12.73	0.00	0.74	1.22	23.31	1.17 *	2.06	0.00	-	558	4.18

* Value calculated based on concentrate modal mineralogy; ** EPMA results normalized due to low totals.

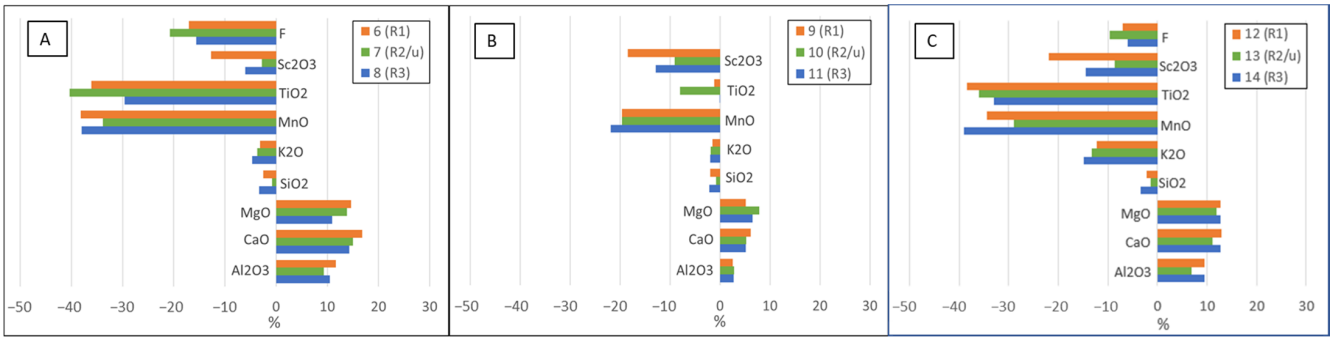

Figure 6. Differences between the analyzed (EPMA) and calculated (ICP-OES) slag compositions. Experiments using concentrates R1, R2/u, and R3 with (**A**) 7% CaF_2, (**B**) 5% CaO, and (**C**) 7% CaF_2 + 5% CaO.

According to the slag and metal EPMA data, reduction of the MnO, TiO_2, K_2O, and SiO_2 components from slag occurred to some extent, particularly with CaF_2 additions. The negative values for Sc_2O_3 are considered to be arising from the challenges in trace element analysis with EPMA and because Sc_2O_3 is thermodynamically very stable in comparison to other components in the slag [30,31]. Back-scattered electron images of the slags and typical structures in large metal accumulations produced from the R3 concentrate with various doping are presented in Figure 7.

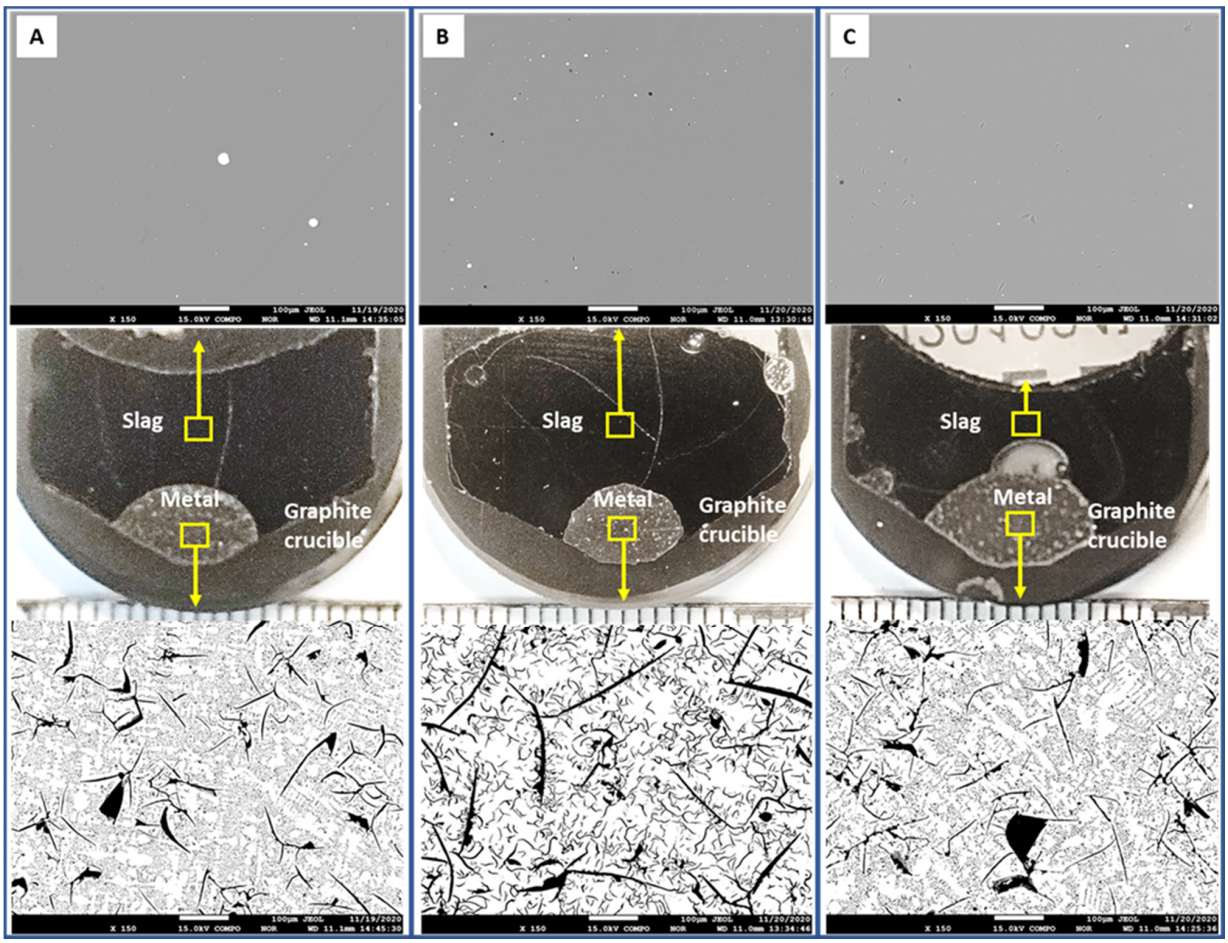

Figure 7. Back-scattered electron images of slag and metal after experiments with concentrate R3 conducted up to 1500 °C with various doping. (**A**) 7% CaF_2, (**B**) 5% CaO, and (**C**) 7% CaF_2 + 5% CaO additions.

There were no significant differences in the amount or size of small metal inclusions in the slag between the experimental runs with CaF_2 and CaO additions. Large graphite-bearing metal accumulations occurred at the bottom of the crucibles with smaller metal droplets on the sides, along the contact of the slag and graphite crucible. The wetting of graphite–slag interfaces by slag without an FeO component has been regarded as rather poor depending on the carbon-slag interfacial tension, slag and carbon surface tension, and the dynamic reactions occurring at the interface [32]. It is apparent from the observed concave slag surface with CaF_2 doping (Figure 7A,C), in comparison to the convex surface with only CaO doping (Figure 7B), that the surface characteristics for these slags are quite different. CaF_2 is known to be a surface-active constituent in slags [21]. In their evaluation of the surface tension of molten ionic mixtures containing CaF_2, Nakamoto et al. [21] stated that in the SiO_2–CaO–CaF_2 system at 1500 °C, the surface tension decreases with increasing CaF_2 content, apparently also applying to the slag system of this study.

Metal analyses revealed similar phases as described in our previous experiments, including eutectic steadite between Si-containing ferrite and flake graphite and/or inter-dendritic graphite segregations. These experiments also exhibited increased silica reduction with CaF_2 doping, which is indicated by an increase in the conversion rates at temperatures of >1450 °C (Figure 5B). In accordance with the previous experiments, titanium carbide (TiC) was detected occasionally at the borders between ferrite and graphite. Averages of the ferrite analyses are provided in Figure 8 with details provided in the electronic supplementary data (Table S2). Graphite crystallization in cast gray iron is a complex phenomenon, which is controlled by melt composition, temperature, and cooling rate [25,33]. According to the textures developed in large metal accumulations, the tendency to form fine inter-dendritic graphite was promoted by a higher silicon content in the metal (Figures 7 and 8). Metallic iron somewhat penetrated the graphite crucible, dissolving carbon into the metal and producing the above-mentioned textures upon cooling. Furthermore, the gas bubble formed on top of the large metal accumulation (Figure 7C) indicated gasification reactions at the Fe–C surface; as proposed by Teasdale and Hayes [34,35], gasification of the carbon in the alloy produces CO as one of the reaction steps involved in the reduction of slag by solid carbon in the presence of liquid Fe-C. As stated by White et al. [36], liquid slags react with carbon in surprisingly complex ways, with liquid Fe-C metal and gas-forming reactions from various slag components contributing to the whole scenario.

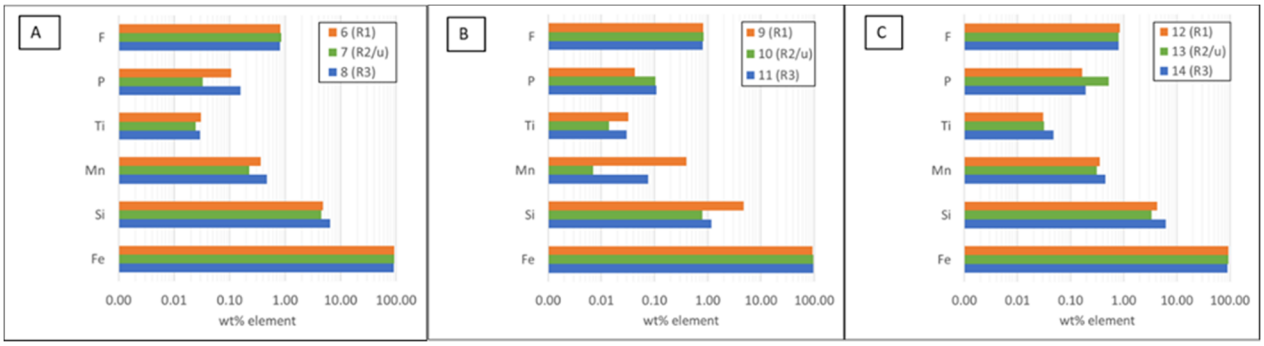

Figure 8. Average ferrite compositions in wt% determined by EPMA in experiments on variously doped concentrates R1, R2/u, and R3. (**A**) 7% CaF_2, (**B**) 5% CaO, and (**C**) 7% CaF_2 + 5% CaO additions.

The design of the type and quantity of doping used in our experiments is based on the ternary Al_2O_3-CaO-SiO_2 phase diagram presented in Figure 9, which exhibits the target area with lower liquidus temperatures as indicated in the close-up. To calculate and plot the compositions on the phase diagram, only the main oxide components (Tables 3, 6 and S2) were considered. Slag compositions based on calculations from both ICP-OES and EPMA data are shown in comparison in Figure 9, which was computed with the FactSage version 7 and its FToxid database.

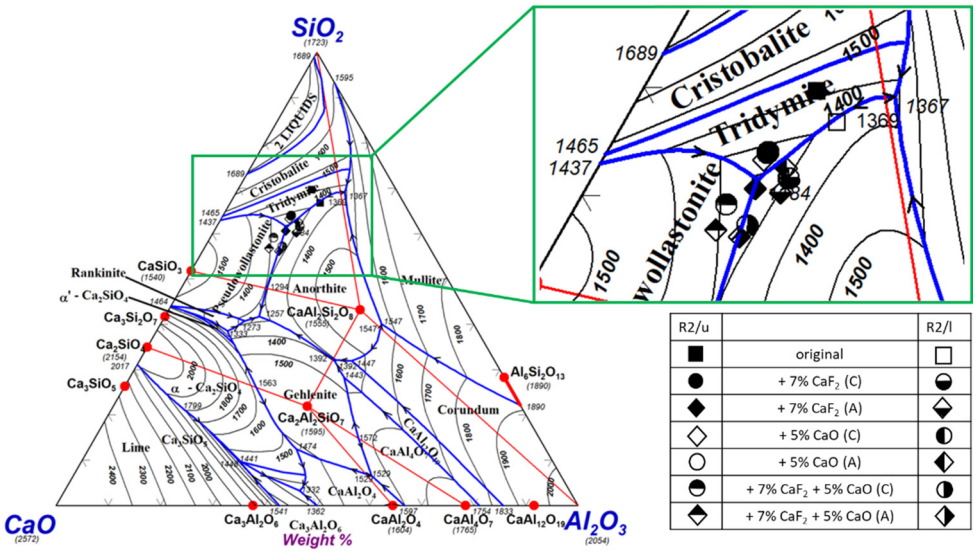

Figure 9. Ternary Al_2O_3-CaO-SiO_2 phase diagram with the target liquidus temperature area (<1300 °C) displayed in the close-up view. Original and modified slag compositions from R2/u and R2/l concentrates computed and plotted with FactSage version 7 and its FToxid database. C = calculated from ICP-OES data and A = calculated from EPMA analysis data.

The amounts of the additions of CaF_2 and CaO were based on the desired liquidus temperature area (<1300 °C) of the system, with the target being close to the ternary eutectic composition. As indicated by the close-up view of the phase diagram area, 7% CaF_2 and 5% CaO were sufficient, resulting in compositions located in the target area in terms of the main components, as confirmed with EPMA data. The commonly expressed empirical slag basicity based on CaO/SiO_2 [15,17] varied in the experiments without doping between 0.20 and 0.24, whereas in the doped experiments, it fell in the range of 0.32–0.54. Even though these values still indicate a very high acidity and therefore a high viscosity, the applied relatively moderate additions of CaF_2 and CaO did improve the properties of the slag by adjusting the composition to the target liquidus temperature area.

3.4. Main Features of the Progression of Reduction at Selected Temperatures with CaO Addition

As the final aspect of our pyrometallurgical studies, the main features of the progression of reduction at selected temperatures (950, 1050, 1150, 1250, and 1350 °C) were investigated with concentrate R3 and 5% CaO addition (Table 1). Based on previous experiments, the differences between CaF_2 and CaO doping are negligible, both improving the slag properties, promoting the reduction of the slag FeO component, and improving the metal segregation. However, CaO would be the likely choice to be used considering environmental aspects and other issues related to the CaF_2 usage. A preliminary experiment was conducted with a gas composition of 95% Ar + 5% H_2 to 1500 °C to provide the baseline against which intercepts at various temperatures could be evaluated. By replacing CO with a mixture of Ar and H_2, the possibility of the reversed Boudouard reaction was eliminated. A comparison of the mass change and conversion rates with 100% CO and 95% Ar + 5% H_2 are provided in the electronic supplementary data (Figure S1). Despite the differences at temperatures of <900 °C, the main stage of ferrous silicate reduction reactions was initiated at the same temperature with both gas flows, peaking at ~1050 °C, with similar final mass changes of 15.19 and 14.88% at 1500 °C for 100% CO and 95% Ar + 5% H_2, respectively. Therefore, the last set of experiments was conducted with a gas flow of 95% Ar and 5% H_2. Details of mass change rates are provided in the electronic supplementary data (Figure S2).

As mentioned in Kallio et al. [9], mass loss curves for such a heterogeneous system as the Kiviniemi concentrate represent a sum of interlapping and interactive phenomena originating from various reactions within and from various types of crystal structures. These include dehydration, dehydroxylation, thermal dissociation, and gas–solid reduction

reactions at lower experimental temperatures, shifting with a rising temperature into melting, slag formation, and gas–liquid and solid–liquid reactions [37,38]. In addition to chemical reactions at reactant–product interfaces, diffusion and heat transfer account for the whole scenario: heat transfer from the furnace to the outer regions of the sample and into the sample, self-cooling, or self-heating of the sample during reactions, removal of evolved gaseous products, and the influence of these products on the rates of reactions all add to the scenario [39]. Despite the complexity of the phenomena, some of the main observed features at selected temperatures are presented and discussed. Figure 10 provides an overview at different temperatures, with photographs of samples and back-scattered electron images plotted on the derivative conversion curve of the baseline experiment.

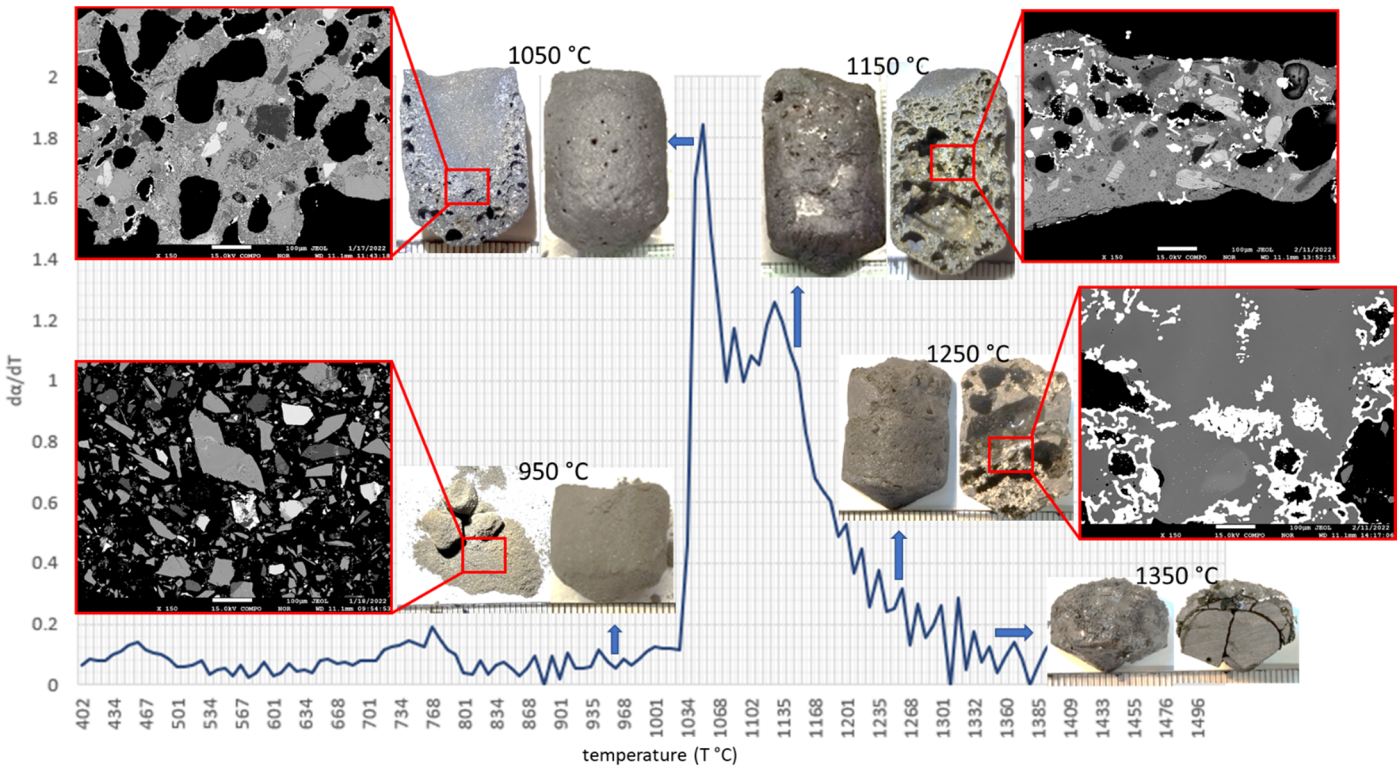

Figure 10. Photographs of samples at different temperatures (950, 1050, 1150, 1250, and 1350 °C), plotted on the derivative conversion curve of the baseline experiment with 95% Ar + 5% H_2. The back-scattered electron images of the samples visualize the progression of mineral decompositions, slag, and metallic iron formation.

For the R3 concentrate, the main reduction stage with a rapid increase in the conversion rates was initiated at ~1030 °C, with highest rates at 1050 °C. Therefore, as expected, the concentrate showed very limited changes at 950 °C. Differences between clinopyroxene and amphibole are visualized in more detail in Figure 11. At 950 °C, clinopyroxene appeared as an intact mineral with the original composition and structure, whereas dehydroxylation and reaction with the reducing gas phase resulted in the destruction of the original amphibole structure and formation of new solid phases, including minuscule metallic iron particles within the relict of an amphibole crystal. XRD patterns in Figure 12 demonstrate the complexity of concentrate crystal structures at 950 °C, with identifiable patterns for potassium feldspar, plagioclase, clinopyroxene, garnet, fayalite, ilmenite, and even amphibole, with relicts occasionally preserved within larger grains.

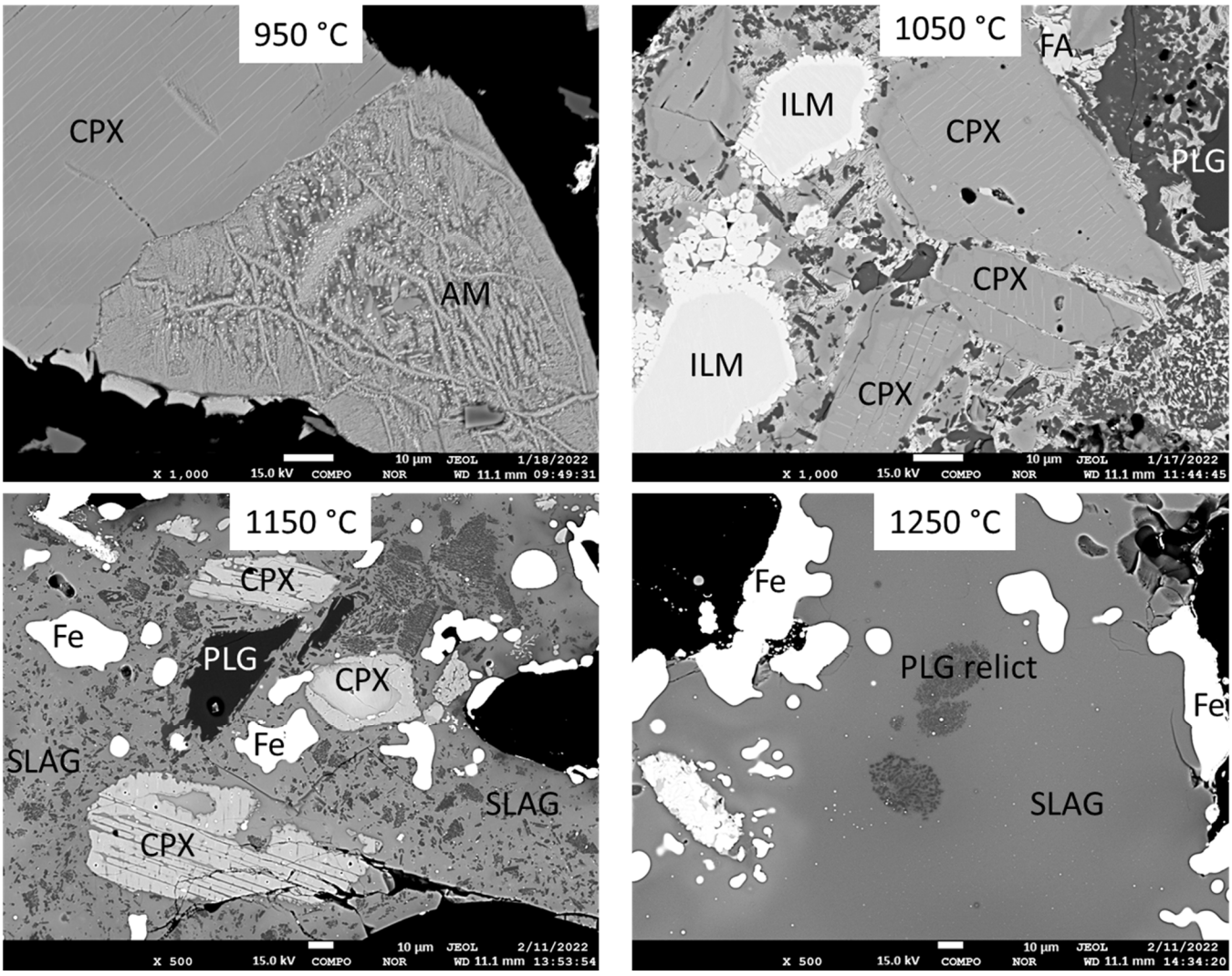

Figure 11. Details of mineral reactions and progression of decomposition with formation of slag and metallic iron at 950, 1050, 1150, and 1250 °C. Mineral abbreviations: CPX = clinopyroxene, AM = amphibole, ILM = ilmenite, FA = fayalite, PLG = plagioclase, Fe = metallic iron.

Increasing the temperature to 1050 °C caused drastic changes in the sample. Particularly along the contact between the concentrate and graphite crucible, the porosity was increased whereas the middle and top parts of the sample exhibited much less porosity, a lower amount of initial slag, and more preserved mineral grains. The height of the sample was increased due to gas-forming reduction reactions, creating porosity, which was formed around graphite particles, producing metal rims around the pores (Figure 10). The formation of initial slag was dominated by the decomposition of amphibole and garnet, sintering the sample into a solid block. The decomposition products of various types of amphiboles have been found to include different phases, such as pyroxene, spinel, olivine, feldspars, and silica in addition to melt [40,41]. Furthermore, the decomposition of garnet under reducing conditions (>1000 °C) has been found to produce metallic iron, cristobalite, and hercynite, with fayalite as a secondary product [42]. In our samples, the common decomposition products observed were very fine-grained mixtures of dark, lath-shaped crystals with a composition resembling plagioclase and FeO-rich phase, with a tendency to form dendrites and/or formation of fayalite as an intermediate decomposition product within the slag phase (Figure 11). The interplay of decomposition products and mineral reactions with evolving slag phase do provide challenges to the interpretation of individual mineral reactions, the details of which could be a subject for further studies. With respect to more

persistent primary minerals at this temperature, such as clinopyroxene, ilmenite, potassium feldspar, and plagioclase, it can be stated that reaction rims, dissolution structures, and zoning are common features, as illustrated in Figure 11. In addition to metallic iron and graphite, clinopyroxene and plagioclase are identifiable in XRD patterns (Figure 12) at this temperature. Details of XRD interpretations are provided in the electronic supplementary data (Figure S3).

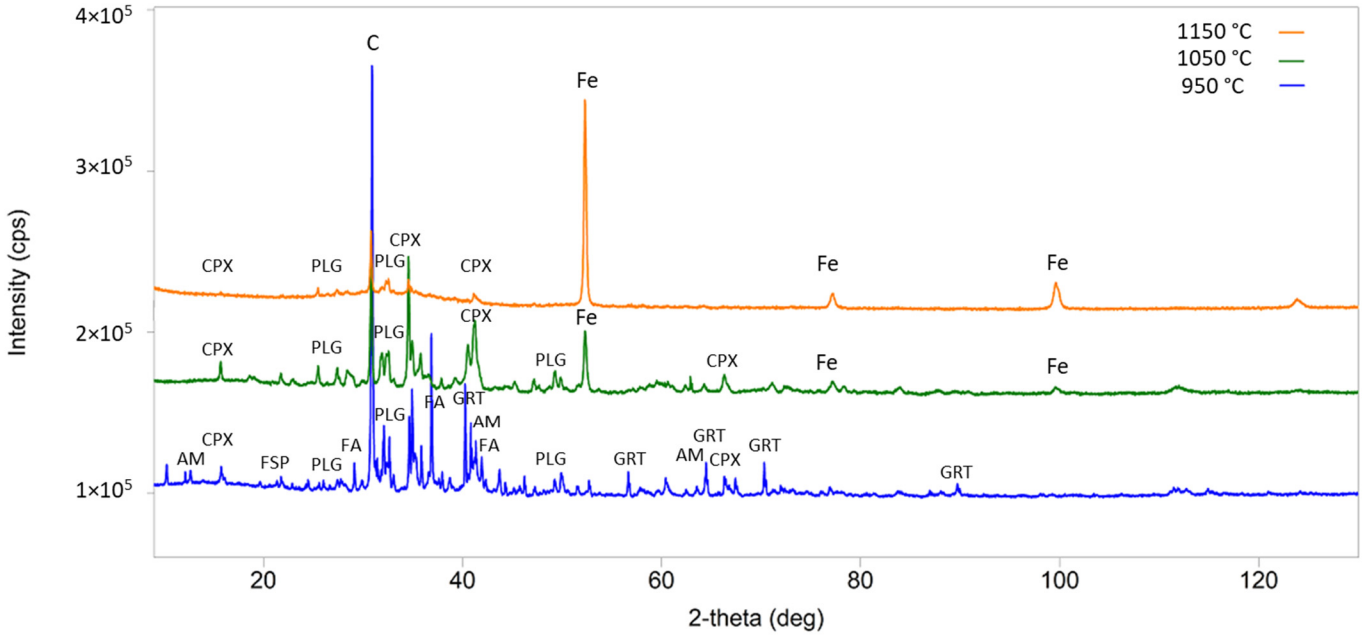

Figure 12. XRD patterns of concentrate R3 reduced at temperatures of 950, 1050, and 1150 °C. Mineral abbreviations: AM = amphibole, CPX = clinopyroxene, FA = fayalite, GRT = garnet, PL = plagioclase, FSP = potassium feldspar, C = graphite, Fe = metallic iron.

At 1150 °C, along the progression of reduction reactions, the amount of metallic iron and slag increased, with the porosity extending throughout the whole sample (Figure 10). Amorphous slag and metallic iron were the dominant phases in XRD patterns, with minor peaks still identifiable for clinopyroxene and plagioclase (Figure 12). By 1250 °C, only occasional plagioclase relicts remained in the slag, as presented in Figure 11, still with an extensive porosity, which is diminished by 1350 °C (Figure 10).

The evolution of the chemical composition of the slag phase is summarized in Figure 13, displaying binary plots of the main components and Sc_2O_3 vs. SiO_2. The analytical results at 950 °C are for amphibole relicts, whereas at other temperatures, the compositions represent those of the slag phase. The slag phase exhibits a steady decrease in FeO due to the progression of reduction with increasing temperature. Based on these results, the slag compositions at 1050 °C with higher CaO content indicate the dissolution of added CaO into the initial slag. As the mineral reactions proceeded with increasing temperature, leading eventually to the decomposition and melting of all clinopyroxene, potassium feldspar, and plagioclase into the slag by 1250 °C, the composition of the slag became homogenized with respect to the main components, with a steady decrease in FeO.

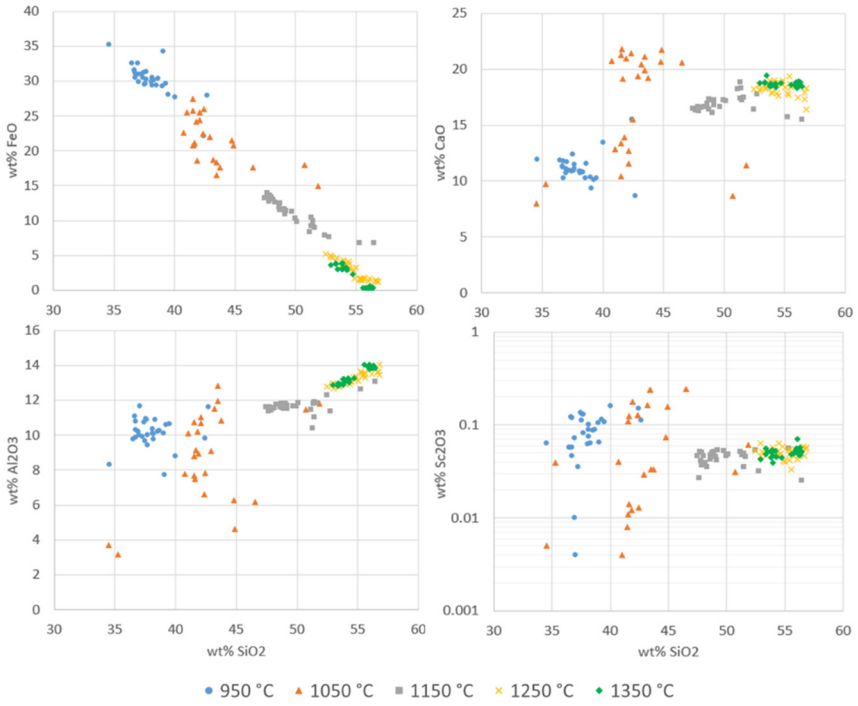

Figure 13. Binary plots of FeO, CaO, Al_2O_3, and Sc_2O_3 (wt%) for amphibole relicts (blue) at 950 °C and slag at higher temperatures.

4. Conclusions

If pyrometallurgical treatment is to be considered for Kiviniemi-type ferrous scandium concentrates, one of the challenges is to optimize and modify the composition of highly viscous slag to promote the reduction of FeO and segregation of metal without excessively diluting the slag Sc_2O_3 content. According to the results of this study, the reduction of the ferrous oxide component of the slag and segregation of metallic iron was improved with moderate additions of CaF_2 and CaO, which lowered the liquidus temperature and viscosity of the slag. The Sc_2O_3 component was maintained and enriched in the slag. Although CaF_2 increased the derivative conversion rates at a slightly lower temperature region, the use of CaO instead of CaF_2 would be preferable in industrial applications. Despite the variations in the modal mineralogy of the concentrate feed used in this study, the high-temperature behavior of the concentrates is essentially similar, though the main reduction stage is initiated at a slightly higher temperature (~1000–1030 °C) for the concentrates with less amphibole and a higher amount of nonferrous gangue minerals. The beginning of the main reduction stage with the formation of initial slag is dominated by the decomposition and reduction of amphibole and garnet. The final decomposition of clinopyroxene, the other main host for Sc_2O_3, occurs at a significantly higher temperature than that of amphibole, with structures persisting until 1150 °C. This study complements the pyrometallurgical part of our ongoing project, confirming the smelting reduction characteristics of the Kiviniemi-type ferrous scandium concentrates. Only after the complete decomposition and melting of silicates and dissolution of unreduced FeO into the slag can the final FeO reduction from slag be achieved by carbon, accompanied by segregation and accumulation of metallic iron.

Supplementary Materials: The following supporting information can be downloaded at: https://www.mdpi.com/article/10.3390/met12050709/s1, Table S1: Modal compositions and deportment of the main components in Kiviniemi concentrates. Table S2: Summary of the metal EPMA analytical data. Table S3: Summary of the first set of slag EPMA analytical data for experiments 6–14. Figure S1: Comparison of the mass change and derivative conversion rates with 100% CO and 95% Ar + 5% H2. Figure S2: Details of mass change rates with 95% Ar + 5% H_2 at various end temperatures. Figure S3: XRD interpretations at selected temperatures.

Author Contributions: Conceptualization, R.K. and P.T.; methodology, R.K., P.T. and E.-P.H.; investigation, R.K. and T.K.; resources, P.T. and T.F.; writing—original draft preparation, R.K.; writing—review and editing, E.-P.H., P.T., S.L. and T.F.; visualization, R.K. and E.-P.H.; supervision, S.L. and T.F.; project administration, T.F.; funding acquisition, R.K. and P.T. All authors have read and agreed to the published version of the manuscript.

Funding: This research has been funded by The Foundation for Research of Natural Resources in Finland, grant number 20210019.

Institutional Review Board Statement: Not applicable.

Informed Consent Statement: Not applicable.

Data Availability Statement: Not applicable.

Acknowledgments: This research has been funded by The Foundation for Research of Natural Resources in Finland. Support and advice from the doctoral training follow-up group members, Jussi Liipo and Tapio Halkoaho, are highly appreciated. The samples from Kiviniemi were provided by the GTK and Metso Outotec enabled the experiments with LIMS and SLon, which are all gratefully acknowledged. The authors are also thankful to Eero Hanski for comments on the manuscript and to CMA personnel for their help with analytical work.

Conflicts of Interest: The authors declare no conflict of interest.

References

1. Hokka, J.; Halkoaho, T. *3D Modelling and Mineral Resource Estimation of the Kiviniemi Scandium Deposit, Eastern Finland*; Mineral Resource Estimation Report; Geological Survey of Finland: Espoo, Finland, 2017; 21p. [CrossRef]
2. Halkoaho, T.; Ahven, M.; Rämö, O.T.; Hokka, J.; Huhma, H. Petrography, geochemistry and geochronology of the Sc-enriched Kiviniemi ferrodiorite intrusion, eastern Finland. *Miner. Depos.* **2020**, *55*, 1561–1580. [CrossRef]
3. Korhonen, T.; Neitola, R.; Mörsky, P.; Laukkanen, J. *Preliminary Beneficiation Study on Kiviniemi Samples*; Report of Investigation; Geological Survey of Finland: Espoo, Finland, 2011; 35p. (In Finnish)
4. Kallio, R.; Tanskanen, P.; Luukkanen, S. Magnetic preconcentration and process mineralogical study of the Kiviniemi Sc-enriched ferrodiorite, eastern Finland. *Minerals* **2021**, *16*, 966. [CrossRef]
5. Wang, W.; Pranolo, Y.; Cheng, C.Y. Metallurgical processes for scandium recovery from various resources: A review. *Hydrometallurgy* **2011**, *108*, 100–108. [CrossRef]
6. Borra, C.R.; Pontikes, Y.; Binnemans, K.; Van Gerven, T. Leaching of rare earths from bauxite residue (red mud). *Min. Eng.* **2015**, *76*, 20–27. [CrossRef]
7. Zhou, K.; Teng, C.; Zhang, X.; Peng, C.; Chen, W. Enhanced selective leaching of scandium from red mud. *Hydrometallurgy* **2018**, *182*, 57–63. [CrossRef]
8. Yagmurlu, B.; Alkan, G.; Xakalashe, B.; Schier, C.; Gronen, L.; Koiwa, I.; Dittrich, C.; Friedrich, B. Synthesis of scandium phosphate after peroxide assisted leaching of iron depleted bauxite residue (red mud) slags. *Sci. Rep.* **2019**, *9*, 11803. [CrossRef]
9. Kallio, R.; Tanskanen, P.; Heikkinen, E.P.; Kokkonen, T.; Luukkanen, S.; Fabritius, T. Reduction characteristics of Kiviniemi ferrous scandium concentrate. *Miner. Eng.* **2022**, *177*, 107369. [CrossRef]
10. Kracek, F.C. *Contributions to Geochemistry: Melting and Transformation Temperatures of Mineral and Allied Substances*; Geological Survey Bulletin 1144-D; U.S. Government Publishing Office (USGPO): Washington, DC, USA, 1963; 88p.
11. Sarma, B.; Cramb, A.W.; Fruehan, R.J. Reduction of FeO in smelting slags by solid carbon: Experimental results. *Metall. Mater. Trans. B* **1996**, *27*, 717–730. [CrossRef]
12. Kondratiev, A.; Jak, E.; Hayes, P.C. Predicting slag viscosities in metallurgical systems. *Jom* **2002**, *54*, 41–45. [CrossRef]
13. Seetharaman, S.; Mukai, K.; Sichen, D. Viscosities of slags—An overview. *Steel Res. Int.* **2005**, *76*, 267–278. [CrossRef]
14. Kekkonen, M.; Oghbasilasie, H.; Louhenkilpi, S. *Viscosity Models for Molten Slags*; Aalto University Publication Series Science + Technology; Department of Materials Science and Engineering, Aalto University: Helsinki, Finland, 2012; 38p.
15. Verein Deustcher Eisenhüttenleute (Ed.) *Slag Atlas*; Verlag Stahleisen M.B.H.: Düsseldorf, Germany, 1981; 282p.
16. Seetharaman, S. (Ed.) *Fundamentals of Metallurgy*; Woodhead Publishing Limited: Sawston, UK; CRC Press: Boca Raton, FL, USA, 2005; 574p.
17. Mills, K.C.; Hayashi, M.; Wang, L.; Watanabe, T. *The Structure and Properties of Silicate Slags. Treatise on Process Metallurgy*; Elsevier: Amsterdam, The Netherlands, 2013; Volume 1, pp. 149–286. [CrossRef]
18. Park, J.H.; Min, D.J.; Song, H.S. Amphoteric behavior of alumina in viscous flow and structure of CaO-SiO_2 (-MgO)-Al_2O_3 slags. *Metall. Mater. Tran. B* **2004**, *35*, 269–275. [CrossRef]
19. Kato, M.; Minowa, S. Viscosity Measurements of Molten Slag. *Transactions ISIJ* **1969**, *9*, 31–38. [CrossRef]
20. Wu, L.; Gran, J.; Sichen, D. The effect of calcium fluoride on slag viscosity. *Metall. Mater. Tran. B* **2011**, *42*, 928–931. [CrossRef]

21. Nakamoto, M.; Tanaka, T.; Holappa, L.; Hämäläinen, M. Surface tension evaluation of molten silicates containing surface-active components (B_2O_3, CaF_2 or Na_2O). *ISIJ Int.* **2007**, *47*, 211–216. [CrossRef]
22. Persson, M.; Seetharaman, S.; Seetharaman, S. Kinetic studies of fluoride evaporation from slags. *ISIJ Int.* **2007**, *47*, 1711–1717. [CrossRef]
23. Wang, H.; Li, G.; Dai, Q.; Lei, Y.; Zhao, Y.; Li, B.; Shi, G.; Ren, Z. Effect of additives on viscosity of LATS refining ladle slag. *ISIJ Int.* **2006**, *46*, 637–640. [CrossRef]
24. Moreira, A.S.B.; Silva, C.A.; Silva, I.A. Replacement of fluorspar in the desulphurization of hot metal. *REM Int. Eng. J.* **2018**, *71*, 261–267. [CrossRef]
25. Radzikowska, J.M. Metallography and Microstructures of Cast Iron. In *ASM Handbook: Metallography and Microstructures*; ASM International: Materials Park, OH, USA, 2004; Volume 9, pp. 565–587.
26. Rout, K.R.; Gil, M.V.; Chen, D. Highly selective CO removal by sorption enhanced Boudouard reaction for hydrogen production. *Catal. Sci. Technol.* **2019**, *9*, 4100–4107. [CrossRef]
27. Batanova, V.G.; Sobolev, A.V.; Magnin, V. Trace element analysis by EPMA in geosciences: Detection limit, precision and accuracy. In *IOP Conference Series: Materials Science and Engineering*; IOP Publishing: Bristol, UK, 2018; Volume 304. [CrossRef]
28. Fialin, M.; Rémy, H.; Richard, C.; Wagner, C. Trace element analysis with the electron microprobe: New data and perspectives. *Am. Mineral.* **1999**, *84*, 70–77. [CrossRef]
29. Vind, J.; Malfliet, A.; Bonomi, C.; Paiste, P.; Sajó, I.E.; Blanpain, B.; Tkaczyk, A.H.; Vassiliadou, V.; Panias, D. Modes of occurrences of scandium in Greek bauxite and bauxite residue. *Miner. Eng.* **2018**, *123*, 35–48. [CrossRef]
30. Gupta, G.K.; Krishnamurthy, N. *Extractive Metallurgy of Rare Earths*; CRC Press: Boca Raton, FL, USA, 2005; Volume 37. [CrossRef]
31. Faris, N.; Ram, R.; Tardio, J.; Bhargava, S.; McMaster, S.; Pownceby, M.I. Application of ferrous pyrometallurgy to the beneficiation of rare earth bearing iron ores—A review. *Miner. Eng.* **2017**, *110*, 20–30. [CrossRef]
32. Siddiqi, N.; Sahajwalla, V.; Ostrovski, O.; Belton, G.R. Wettability of graphite by CaO-SiO_2-Al_2O_3-FeO-MgO slag. *High Temp. Mater. Process* **1997**, *16*, 213–225. [CrossRef]
33. Stefanescu, D.M.; Alonso, G.; Larrañaga, P.; De la Fuente, E.; Suarez, R. A comparative study of graphite growth in cast iron and in analogous systems. *Int. J. Met.* **2018**, *12*, 722–752. [CrossRef]
34. Teasdale, S.L.; Hayes, P.C. Observations of the reduction of FeO from slag by graphite, coke and coal char. *ISIJ Int.* **2005**, *45*, 634–641. [CrossRef]
35. Teasdale, S.L.; Hayes, P.C. Kinetics of reduction of FeO from slag by graphite and coal chars. *ISIJ Int.* **2005**, *45*, 642–650. [CrossRef]
36. White, J.F.; Lee, J.; Hessling, O.; Glaser, B. Reactions between liquid CaO-SiO_2 slags and graphite substrates. *Metall. Mater. Trans. B* **2017**, *48*, 506–515. [CrossRef]
37. Foldvari, M. *Handbook of Thermogravimetric System of Minerals and Its Use in Geological Practice*; Geological Institute of Hungary: Budapest, Hungary, 2011; Volume 213, 180p.
38. Saadatkhah, N.; Carillo Garcia, A.; Ackermann, S.; Leclerc, P.; Latifi, M.; Samih, S.; Patience, G.S.; Chaouki, J. Experimental methods in chemical engineering: Thermogravimetric analysis—TGA. *Can. J. Chem. Eng.* **2020**, *98*, 34–43. [CrossRef]
39. Brown, M.E. *Introduction to Thermal Analysis*; Kluwer Academic Publishers: Dodrecht, The Netherlands, 2004; 264p.
40. Brett, N.H.; Mackenzie, K.J.D.; Sharp, J.H. The thermal decomposition of hydrous layer silicates and their related hydroxides. *Q. Rev. Chem. Soc.* **1970**, *24*, 185–207. [CrossRef]
41. Grapes, R. *Pyrometamorphism*, 2nd ed.; Springer: Berlin, Germany, 2006; 365p.
42. Aparicio, C.; Filip, J.; Mashlan, M. High temperature decomposition of almandine and pyrope in reducing atmosphere. In *AIP Conference Proceedings*; American Institute of Physics: College Park, MD, USA, 2010; Volume 1258, pp. 47–54. [CrossRef]